Author Manuscript

Author Manuscript

Author Manuscript

Author Manuscript

HHS Public Access

Author manuscript

Anal Chem. Author manuscript; available in PMC 2019 October 16.

Published in final edited form as:

Anal Chem. 2018 October 16; 90(20): 11863–11872. doi:10.1021/acs.analchem.8b01881.

In Vivo Stable Isotope Labeling and Mass Spectrometry-Based Metabolic Profiling of a Potent Tobacco-Specific Carcinogen in Rats

Romel Dator[1], **Linda B. von Weymarn**[1], **Peter W. Villalta**[1], **Cory J. Hooyman**[2], **Laura A. Maertens**[1], **Pramod Upadhyaya**[1], **Sharon E. Murphy**[1], **Silvia Balbo**[1,*]

[1]Masonic Cancer Center, University of Minnesota, 2231 6th Street SE, Minneapolis, MN 55455

[2]Independent Consultant, 3732 Harriet Avenue S., Minneapolis, MN 55409

Abstract

The tobacco-specific nitrosamine, 4-(methylnitrosamino)-1-(3-pyridyl)-1-butanone (NNK), is a potent lung carcinogen and exerts its carcinogen effects upon metabolic activation. The identification and quantitation of NNK metabolites could identify potential biomarkers of bio-activation and detoxification of this potent carcinogen and may be used to predict lung cancer susceptibility among smokers. Here, we have used *in vivo* isotope labeling and high-resolution mass spectrometry-based methods for the comprehensive profiling of all known and unknown NNK metabolites. The sample enrichment, LC/MS, and data analysis workflow, including the custom script for automated d_0-d_4 *m/z* pair peak detection, enabled unbiased identification of numerous NNK metabolites. The structures of the metabolites were confirmed using targeted LC-MS^2 with retention time (t_R) and MS^2 fragmentation comparison to standards when possible. Eleven known metabolites and the unchanged NNK were identified simultaneously. More importantly, our workflow revealed new and novel NNK metabolites including: the 1,3-Diol (**13**); α-OH-methyl-NNAL-Gluc (**14**); nitro-NK-*N*-oxide (**15**); nitro-NAL-*N*-oxide (**16**); γ-OH NNAL (**17**); and three N-acetylcysteine (NAC) metabolites (**18a-c**). We measured the differences in the relative distribution of a panel of nitroso-containing NNK-specific metabolites in rats before and after phenobarbital (PB) treatment, and this serves as a demonstration of a general strategy for the detection of metabolic differences in animal and cell systems. Lastly, we have generated a d_4-labeled NNK metabolite mixture to be used as internal standards (d_4-rat urine) for relative quantitation of NNK metabolites in humans, and this new strategy will be used to assess carcinogen exposure and ultimately to evaluate lung cancer risk and susceptibility in smokers.

Keywords

NNK; tobacco carcinogens; metabolites profiling; mass spectrometry; stable isotope labeling

*To whom correspondence should be addressed. Phone: (612) 624-4240, Fax: (612) 624-3869, balbo006@umn.edu.

Supporting Information Available

Supporting Information. Excel spreadsheets containing datasets from U1*, U2*, U3*, and BU* (Table S1–Table S5), custom script for the automated peak pair detection, and PDF file with Figure S1–S10 and Table S6–Table S11. The information is available free of charge via the Internet at http://pubs.acs.org/.

Author Manuscript Author Manuscript Author Manuscript Author Manuscript

INTRODUCTION

Lung cancer is the most common and preventable form of cancer worldwide. In the United States, it is the leading cause of cancer mortality among men and women, and in 2017 it was estimated that 1 out of 4 cancer deaths were due to lung cancer.[1] The strong correlation between lung cancer and tobacco smoking is well documented, however, despite the 90% lung cancer incidence caused by tobacco smoking, only a small fraction (11–24%) of smokers will develop the disease over their lifetime.[2,3] It is hypothesized that this disparity may be due to inter-individual genetics differences, which result in variations in the uptake and metabolism of tobacco carcinogens leading to differing levels of carcinogen-derived metabolites.[4–6] The quantitation of these metabolites could provide insights into the relative contributions of the different pathways involved in the bio-activation and detoxification of carcinogens, and could enable rational strategies for cancer prevention based on targeted surveillance of high-risk and susceptible populations.

4-(Methylnitrosamino)-1-(3-pyridyl)-1-butanone (NNK) is a potent lung carcinogen present in all tobacco products and one of the most powerful carcinogens in tobacco smoke. It is classified as a Group 1 human carcinogen by the International Agency for Research on Cancer. In order to exert its carcinogenic effects, NNK must be metabolically activated into highly reactive species capable of modifying DNA. These modifications may result in DNA damage that, if not repaired, can lead to mutations causing cell growth dysregulation and cancer.

Previous studies have extensively characterized the metabolic pathways of bio-activation and detoxification of NNK in laboratory animals.[7–12] Figure 1 summarizes the structures of known NNK metabolites as determined in animal models. NNK is primarily metabolized by *N*-oxidation, α-hydroxylation, and carbonyl reduction to 4-(methylnitrosamino)-1-(3-pyridyl)-1-butanol (NNAL), also a potent carcinogen, which is detoxified by conversion to its glucuronide conjugates. Profiling of NNK metabolites has been previously reported using tritium labeled [5-^{3}H]-NNK and radio flow high-performance liquid chromatography (HPLC).[13–19] Using this approach, the retention times of metabolites were compared with the retention times of synthetic standards for qualitative confirmation. While useful in identifying major NNK metabolites, this approach lacks the selectivity for the identification of co-eluting metabolites and does not provide structural information for the characterization of unknown metabolites. The quantitation of some of the identified metabolites have been used to measure carcinogen exposure, uptake, activation, and detoxification in humans. For instance, NNAL and its glucuronides (NNAL-O-Gluc and NNAL-N-Gluc) have been extensively used to measure NNK exposure and detoxification, respectively.[20–22] However, these methods rely on the quantitation of a few predetermined NNK metabolites with known MS fragmentation spectra, and the resulting measurements do not allow for the determination of the relative contributions of the different metabolic pathways responsible for NNK-induced carcinogenesis. A comprehensive method that is able to identify potentially all metabolites and understand the contribution of the various pathways of NNK metabolism is needed.

Author Manuscript Author Manuscript Author Manuscript Author Manuscript

Mass spectrometry-based metabolomics have been extensively used for profiling metabolites resulting from various perturbations in biological systems. Isotope labeling approaches have also been incorporated into these assays, allowing for confident identification and improved quantitation of metabolites. As a result, a number of stable isotope labeling (SIL)-assisted software tools have been developed for untargeted metabolomics, however, most of these tools have been designed for specific applications, which use various labeling and measurement strategies.[23–28] Here, we have developed a workflow to complement these existing tools for processing high-resolution LC/MS mass spectral data obtained from stable isotope labeling experiments. The sample enrichment, LC/MS, and data analysis workflow presented in this work, including the custom script for the automated d_0-d_4 *m/z* pair peak detection, enabled unbiased identification of numerous metabolites, including the identification of new and novel NNK metabolites in rats. Chemical structures for the previously unidentified NNK metabolites are proposed, several of which were expected but had not been detected yet in either animal or human model systems. This new panel of metabolites could serve as potential biomarkers to assess NNK uptake, metabolic activation and detoxification, and ultimately contribute to our understanding lung cancer risk and susceptibility among smokers.

MATERIALS AND METHODS

Caution:

d_0-NNK, d_4-NNK, $^{13}C_6$-NNAL, and NNAL are carcinogens and must be handled carefully and with adequate precautions.

Materials.

F344 rats (Male, 250–300 g) were obtained from Charles River (Kingston, NY). NNAL, [$^{13}C_6$]-NNAL (1,2',3',4',5',6'–$^{13}C_6$), NNAL-O-Gluc, d_0-NNK, d_4-NNK (pyridine-d_4; isotopic purity > 98%), and 1,4-Diol were obtained from Toronto Research Chemicals (TRC, Ontario, Canada). NNK-*N*-oxide, NNAL-*N*-oxide, β-OH NNAL, β-OH NNK-*N*-oxide, 1,3-Diol, HPBA, and OPBA were synthesized as previously described.[11] β-OH NNK was a kind gift from Dr. Stephen Hecht. Oasis HLB and Oasis MCX solid-phase extraction cartridges were purchased from Waters (Milford, MA). Strata-X polymeric reverse-phase cartridge was purchased from Phenomenex (Torrance, CA). All acids and organic solvents were HPLC or MS grade.

In vivo stable isotope labeling of NNK metabolites.

d_0-NNK and d_4-NNK were used to treat F344 rats following a protocol approved by the Institutional Animal Care and Use Committee (IACUC) of the University of Minnesota. Figure 2a illustrates the experimental design for the animal experiment and the four urine samples collected corresponding to the different urine collections (BU, U1, U2, and U3). Baseline urine samples (BU) were collected for 24 hours before the NNK treatment. After which, rats were dosed with an intraperitoneal (i.p.) injection of d_0-NNK (0.1 mg/kg) to Rat A and d_4-NNK to Rat B. Then 24-h urine samples (U1) were collected. To account for individual variability, a cross-over experiment was performed on the next day where d_0-NNK was administered to Rat B and d_4-NNK to Rat A. The 24-h urine samples (U2) were

Author Manuscript Author Manuscript Author Manuscript Author Manuscript

again collected. To enhance the formation and identification of NNK metabolites in rat urine, phenobarbital (PB) (40 mg/kg per day) was administered for three days. PB induces α-hydroxylation of NNK and various UDP-glucuronosyl transferases (UGTs).[15] Following the three-day induction, another i.p. injection of d_0-NNK to Rat A and d_4-NNK to Rat B was administered and urine samples (U3) were collected for 24 hours. All urine samples were collected on cooling blocks to prevent degradation of metabolites and to prevent bacterial growth. A 1:1 (v/v) of each urine sample collection were combined to yield BU*, U1*, U2*, U3*, which were used for the NNK metabolites profiling (Figure 2a).

Rat urine sample preparation.

The sample cleanup and enrichment protocols were optimized using a mixture of synthetic standards consisting of NNAL, [$^{13}C_6$]-NNAL, NNAL-O-Gluc, NNK-*N*-oxide, NNAL-*N*-oxide, 1,4-Diol, HPBA, and OPBA. The methods were further refined using a 1:1 ratio (v/v) of d_0-labeled PB-induced rat urine ($U3_A$) and d_4-labeled PB-induced rat urine ($U3_B$) and monitoring for known NNK metabolites. During the refinement, a protein precipitation step was introduced to eliminate potential interference of high abundant proteins during LC/MS analysis. One hundred (100 μL) microliters of PB-induced d_0-NNK rat urine ($U3_A$) and 100 μL PB-induced d_4-NNK rat urine ($U3_B$) samples were combined. The urine sample was spiked with labeled NNAL ($^{13}C_6$-NNAL, 0.5 pmol) and deproteinized by adding 4 volumes of 1:1:1 acetonitrile (ACN): methanol (MeOH): acetone. The mixture was vortexed and incubated for 15 min on ice. After which, the sample was centrifuged, the supernatant collected and dried under vacuum. The sample was subjected to a series of solid phase extraction systems, with different modes of separation (see Figure S9b for detailed protocol). Figure 2b shows the flow chart of the optimized sample preparation and cleanup strategy used for the LC/MS analyses of rat urine samples.

LC/MS parameters.

All LC/MS experiments were performed on a Thermo Orbitrap Fusion mass spectrometer (Thermo Scientific, Waltham, MA) coupled to a Dionex RSLC UPLC (Thermo Scientific, Sunnyvale, CA). Reverse phase chromatography was performed on a home-packed Luna C18 column (5 μm, 120 Å, 200 mm x 75 μm ID, Phenomenex, Torrance, CA) at room temperature and flow rate of 0.3 μL min^{-1} using 5 mM ammonium acetate as mobile phase A and methanol as mobile phase B. The LC gradient started with 5% B for the first 5 min with a flow rate of 1.0 μL min^{-1}, followed by switching of the injection valve to remove the 5 μL loop from the flow path, and reducing the flow rate to 0.3 μL min^{-1} over 1 minute. A linear gradient from 5% to 98% B over 19 min was used followed by a constant 98% B for 3 min. Finally, re-equilibration was performed by changing the mobile phase composition from 95% to 5% B over 2 min and increasing the flow rate to 1.0 μL min^{-1} over 2 min with a 5% B hold for 6 min. The total run time was 38 min. An optimal S-Lens RF setting of 60% was used for analysis. Instrument sensitivity and mass accuracy was checked using a mixture of synthetic NNK metabolites standard before all LC/MS analyses. Mass spectra were recorded in positive ion mode with nano-electrospray voltage set to 2.2 kV and an ion transfer tube temperature of 350 °C. All LC/MS analyses were operated with at least 30,000 mass resolving power (FWHM) with internal mass calibration using the EASY-IC feature of the Orbitrap Fusion.

Author Manuscript Author Manuscript Author Manuscript Author Manuscript

Untargeted MS-based method for screening known and unknown NNK metabolites in rats.

An untargeted MS-based approach was used for the comprehensive profiling of known and unknown NNK metabolites in the four rat urine samples corresponding to the four urine collections (BU, U1, U2, and U3) as shown in Figure 2a. For each collection, urine from Rat A and Rat B was combined in a 1:1 (v/v) ratio and processed using the sample cleanup protocol shown in Figure 2b. This was done to have both d_0-and d_4-metabolites in each sample, except for the baseline urine (BU). Pairs of d_0-and d_4-NNK metabolites in each of the four samples were then measured during LC/MS analysis using high-resolution full scan data acquisition at a mass range of *m/z* 150–900. The LC/MS and data-analysis workflow for the untargeted profiling for all known and unknown NNK metabolites is illustrated in Figure 3a. The following MS parameters were used for the high-resolution accurate mass full scan data acquisition: mass range, *m/z* 150–900; resolution setting, 240,000; quadrupole isolation; AGC target setting, 4e5; maximum injection time, 100 ms; and RF lens, 60%. The full scan mass spectral data were acquired in centroid mode and analyzed with Compound Discoverer (CD) 2.0 (Thermo Scientific, Sunnyvale CA) to provide feature detection, which further processed following the data analysis workflow shown in Figure 3a. Feature detection in CD was performed using the following parameters: retention time alignment using the adaptive curve alignment model; 5 ppm mass tolerance; 0.2 min retention time tolerance; intensity tolerance of 30% (relative intensity tolerance used for isotope search); S/N threshold of 3; minimum peak intensity of 500; ions detected as $[M+H]^+$, $[M+NH_4]^+$, $[M+Na]^+$, $[M+K]^+$, $[M+H+MeOH]^+$, $[2M+H]^+$, $[M+2H]^{2+}$; minimum element counts (C H); maximum element counts (C_{90}, H_{190}, Br_3, Cl_4, K_2, N_{10}, Na_2, O_{15}, P_2, S_5). The resulting features were exported to Excel (Microsoft) and analyzed for automatic d_0-d_4 *m/z* pair identification using a custom JAVA script implemented on the Google spreadsheet platform, and available at https://docs.google.com/spreadsheets/d/1YN8xwjhylBRloBxMKqau_eAqVHX1FHvpCC7cadzzn3I/edit?ts=5962dd1f#gid=0. The script identifies pairs of features with *m/z* values separated by exactly 4.0251 Da (±0.001 Da). Further analysis is performed to identify those *m/z* pairs that have retention times within 0.2 min, and pairs in samples U1*, U2*, and U3* combined into a single list, which is further scrutinized by: (1) elimination of *m/z* pairs detected in the baseline urine (BU*) sample, (2) manual evaluation of candidate d_0-d_4 pairs using Xcalibur 3.0 (Thermo Scientific, Sunnyvale, CA) to ensure similar peak shape and intensity, and (3) elimination of redundant features by removing multiple instances of *m/z* pairs. The resulting candidate d_0-d_4 *m/z* pairs are assigned to known metabolites based on their accurate masses as determined from the high-resolution full scan data. For those *m/z* pairs which do not correspond to a known metabolite, the measured high-resolution accurate d_0 *m/z* mass is searched against the METLIN database (Scripps, CA) for putative metabolite identification.[29] Both the tentatively assigned NNK metabolites and unknown ones were further confirmed and characterized using targeted LC-MS^2 as described below.

Targeted MS-based approach (structural confirmation).

To gain structural confirmation, the list of *m/z* pairs detected with the untargeted MS-based profiling approach were used to create a targeted mass inclusion list for LC-MS^2 analysis (Figure 4), with reinjection of the samples using the following parameters: quadrupole isolation window; 1.5 *m/z*; HCD (High-energy collisional dissociation); 25%; Orbitrap

Author Manuscript Author Manuscript Author Manuscript Author Manuscript

resolution setting, 30,000; scan range, *m/z* 80–500; RF lens, 60%; AGC target, 5e4; maximum injection time, 54 ms; all parallelizable injection time feature, enabled. The MS^2 data were acquired in profile mode with the EASY-IC internal mass calibration feature enabled. The high-resolution accurate masses of fragment ions of expected and known NNK metabolites were extracted from the MS^2 mass spectral data within 5 ppm mass tolerance. For accurate and confident identification of candidate *m/z* pair, manual evaluation of candidate d_0-d_4 pairs using Xcalibur 3.0 (Thermo Scientific, Sunnyvale, CA) was performed to ensure that the *m/z* pairs have similar peak shape, intensity ratio (d_0/d_4), and have at least 2–3 MS^2 fragment ions for both *m/z* values. Where possible, the retention time and MS^2 fragmentation pattern of synthetic standards were used to confirm the identity of NNK metabolites.

RESULTS AND DISCUSSION

Profiling of NNK metabolites in biological fluids from animals has been traditionally accomplished using tritium labeling and radio flow high-performance liquid chromatography (HPLC). [13–19] In addition, methods based on mass spectrometry, often with selected reaction monitoring (SRM) have been used to quantify selected NNK metabolites in both animal models and humans.[20,21,30–32] While useful in measuring a few NNK metabolites at a time, these methods do not provide structural information for identification and characterization of unknown compounds. Since, the traditional SRM approach measures only a few metabolites per analysis, limited insights are gained on the relative contributions of the individual metabolic pathways to NNK bioactivation and detoxification. Here, we have developed a sample enrichment strategy, HR-AM LC/MS method, and data analysis workflow for the untargeted profiling and simultaneous characterization of known and unknown NNK metabolites. To obtain a comprehensive profile of all NNK metabolites in rats, we analyzed the urine samples of rats treated with d_0-NNK and d_4-NNK.

Untargeted MS-based method for screening known and unknown NNK metabolites in rats.

A sample processing and data analysis workflow was developed to screen for previously characterized NNK metabolites as well as to simultaneously identify new metabolites in rat urine from a d_0- d_4-NNK exposure experiment. We have tested different combinations of SPE columns to provide orthogonal modes of cleanup and enrichment of the different NNK metabolites in the urine sample, and found that the combination of the three SPEs as presented in the manuscript gave the best detection and recovery of most of the known NNK metabolites. For example, using $^{13}C_6$-NNAL spiked into baseline rat urine (1:1 ratio of urine from Rat A and Rat B), the recovery obtained was 73%. The optimized sample preparation method was further refined and applied to the analysis of urine from NNK treated rats (Figure 2a,b). PB treatment was used to induce cytochrome P450 2B (the catalyst of NNK alpha-hydroxylation), and UDP-glucuronosyltransferases.[13,15] To generate a comprehensive NNK metabolism profile of known and unknown NNK metabolites, LC/MS analysis was carried out on 1:1 mixtures of urine samples from two rats (A and B). Four urine samples corresponding to different urine collections were collected from each rat (Figure 2a). Baseline urine (BU) samples were collected on Day 1 before NNK treatment. U1 urine was collected on Day 2 wherein Rat A was treated with d_0-NNK and Rat B with d_4-NNK. On

Author Manuscript Author Manuscript Author Manuscript Author Manuscript

Day 3, the exposures were switched, and Rat A received d_4-NNK and Rat B received d_0-NNK and urine was again collected for 24 h (U2). This cross-over experiment was performed to account for the biological variability in the metabolism of NNK in the two rats. Lastly, urine samples (U3) were collected on Day 7 after the 3-day PB-treatment and final NNK treatment, where Rat A received d_0-NNK and Rat B d_4-NNK.

The data analysis workflow used for the untargeted profiling of NNK metabolites in rats is illustrated in Figure 3a. The urine from Rat A and B was combined for each urine collection (Figure 2a) to obtain three samples containing both d_0 and d_4-NNK: U1*, U2*, and U3*. The analysis of the three treated samples generated a combined total number of 63,913 features or *m/z* values after feature extraction using Compound Discoverer (~21,000 features detected in each sample) (Table S1). The 63,913 features include features that are common in all three samples as well as features that are unique to each sample. Peak area filtering of features with ion abundance greater than 10,000 yielded 42,389 *m/z* values, which were then uploaded, along with corresponding retention times and peak areas, and analyzed using the automated d_0-d_4 *m/z* pair identification script implemented on a Google spreadsheet platform (Table S2). The custom script was used to select pairs of *m/z* values separated by 4.0251 Da (±0.001 Da), the mass difference expected for the d_0- and d_4-NNK metabolite pairs. This resulted in 6,059 *m/z* pairs (~2,000 in each sample, Table S3). The data were further filtered by an initial retention time (t_R) window of 12 s or 0.2 min to yield a total of 172 d_0-d_4 *m/z* pairs for U1*, U2*, and U3* (Table S4). Fifty (50) non-redundant d_0-d_4 *m/z* pairs were obtained upon subtraction of *m/z* pairs detected in the baseline urine (BU) sample (Table S5), manual evaluation of each *m/z* pair using Xcalibur to ensure that the peak shape and intensity ratio of the d_0-d_4 signals are similar, and exclusion of redundant metabolites or features with similar *m/z* and t_R that are found in at least two urine sample dataset. Redundant metabolites or features are those detected in more than one data set. For instance, NNAL (**2**), was detected in all samples, U1*, U2*, and U3* but was counted only as one of the metabolites in the final 50 d_0-d_4 *m/z* pairs (Table S6).

From the 50 d_0-d_4 *m/z* pairs, 10 metabolites were tentatively identified based on the agreement of the measured accurate masses with those of NNK metabolites previously reported in literature (Table S7). A representative EIC of NNAL (**2**), a major NNK metabolite, from the full scan mass spectral data is presented in Figure 3b. Both d_0-NNAL (*m/z* 210.1238) and d_4-NNAL (*m/z* 214.1488) are present with similar retention times (d_4-NNAL, 15.9 min; d_0-NNAL, 16.0 min). The two peaks observed for both masses correspond to the (*E*)- and (*Z*)- isomers of NNAL. The MS spectrum of these peaks contained pairs of *m/z* values separated by 4.0251 Da (±0.001 Da), *m/z* 210.1238 and *m/z* 214.1488 corresponding to the d_0-NNAL and d_4-NNAL, respectively (Figure 3c). Although full scan data acquisition is not as sensitive as the targeted approach, we were able to simultaneously identify 9 of 11 known metabolites of NNK and the unchanged NNK (Figure 1, Table S7).

Targeted MS-based method for structural confirmation of known metabolites and characterization of new and novel NNK metabolites.

In order to confirm the identity of the 10 tentatively assigned d_0-d_4 *m/z* pairs detected in the untargeted approach (Table S7) and to characterize the remaining 40 pairs, the samples were

Author Manuscript Author Manuscript Author Manuscript Author Manuscript

re-injected for targeted LC-MS^2 structural confirmation (Figure 4). LC-MS^2 analysis of 53 total target pairs, including three additional pairs of NNK metabolites, was performed and fragment ions were extracted. The two undetected NNK metabolites were 6-OH NNK (**5**) and HPB (**9**). One additional mass pair, *m/z* 242.1135 (**16**) and *m/z* 246.1386, was included since a relatively abundant tentative d_0-NNK metabolite, *m/z* 240.0978 (Table 1**, 15**) was observed in the untargeted approach. We hypothesized that a reduced version, which would be a metabolite of NNAL (*m/z* 242.1135) may also be formed. The complete list of the 53 *m/z* pairs used for the LC-MS^2 assay are listed in Table S8.

For accurate and confident identification of NNK metabolites in the targeted LC-MS^2, high-resolution accurate masses of the fragment ions were extracted from the MS^2 data. The following criteria were used to characterize the metabolites, (1) the identified metabolites should have both d_0 and d_4 separated by 4.0251 (±0.001 Da) with a t_R difference of less than 0.2 min, (2) the *m/z* error of the precursor and fragment ions should be less than 5 ppm for both labeled and unlabeled versions, (3) at least 2 or 3 fragment ions separated by 4.0251 (±0.001 Da) should be present in the MS^2 of the d_0-d_4 *m/z* pairs, (4) both labeled and unlabeled analytes should form similar adducts (H, Na, NH_4), and (5) should not be present in the baseline urine, BU* (without NNK treatment). Using the LC-MS^2 analysis for structural confirmation, the 53 d_0-d_4-*m/z* pairs were classified as (a) confirmed metabolites, (b) new proposed metabolites, (c) unknown metabolites (d) in-source decay products (ISD), adducts, and artefacts, and (e) ion clusters and dimers (Table 1 and Table S11).

The identities of the 9 tentatively assigned metabolites and the unchanged NNK (10 total, Table S7) from the untargeted screening approach were confirmed based on their MS^2 fragmentation, t_R comparison with synthetic standards, and from available data in the literature. Two known NNK metabolites, 6-OH NNK (**6**) and HPB (**8**), that were not observed in the untargeted screening were identified using the targeted approach (Table 1). One potential limitation of the current approach is that, due to the position of the deuterium atoms on the NNK, metabolites having the pyridine ring substitution could not be identified. For instance, 6-OH NNK (**5**) was not identified in the screening approach since the metabolite contains only three deuteriums. Because it is a known NNK metabolite, we have added this compound in the targeted LC-MS^2 analysis to confirm its presence in the rat urine. Our approach could be improved by the use of ^{13}C-labeled precursors, but the availability of these labeled compounds is limited and very expensive.

In summary, we have definitively confirmed the presence of NNK and 11 of its metabolites in the urine of F344 rats treated with NNK. In addition to the confirmed metabolites, our workflow revealed new and novel NNK metabolites not previously reported (Table 1). The identities and structures for eight of the unknown *m/z* pairs were proposed based on their high-resolution accurate masses and MS^2 mass spectra, NMR data when possible, and data in the literature. These metabolites included the 1,3-Diol (**13)**; α-OH-NNAL-Gluc (**14**); nitro-NK-*N*-oxide (**15**); nitro-NAL-*N*-oxide (**16**); γ-OH NNAL (**17**); and three N-acetylcysteine (NAC) metabolites (**18a, 18b, 18c**), which were identified, for the first time as NNK metabolites in the rat. The characterization of these metabolites is described in detail below. Three additional potential metabolites were detected, but data supporting their identification is limited (Table 1).

Author Manuscript Author Manuscript Author Manuscript Author Manuscript

Characterization of new and novel NNK metabolites.

Using the *in vivo* d_0-d_4-NNK labeling strategy for the comprehensive characterization of NNK metabolites in rats, we were able to detect and identify new and novel NNK metabolites. The structures and identities of eight of these metabolites were proposed based on high-resolution accurate masses of both precursor ions and MS^2 fragment ions, and comparison to related compounds (Table 1). The 1,3-Diol **(13)** was confirmed as a metabolite of NNK in the rat for the first time here (Figure 5 and Table 1). This compound has previously been identified as a solvolysis product of model compounds that generate the pyridylhydroxybutylating diazohydroxide.[33] The data supporting this is as follows: three chromatographic peaks with *m/z* of 168.1019 and *m/z* 172.1270 pairs were detected (Figure S1a, b). The first, t_R: 14.3 min co-elutes with and has the identical MS^2 spectra as the standard of the 1,4-Diol (Figure 1, **12** and Figure S1 a,b,g,h). Whereas, the peak at t_R: 15.6 min has an identical t_R and MS^2 spectra to the 1,3-Diol (Figure 5, **13**; Figure S1a,b,d,i–k). The third peak with t_R: 16.5 min (Figure S1a,b,e,f), which appears to be another diol (Table 1, **19)** has an MS^2 spectra consistent with a structure where the hydroxyl groups are attach on the same carbon (Figure S1e, f). Although it is typical for geminal diols to lose water and form more stable ketones, in this particular case, this feature seems to lose $^{\bullet}OH$ radical forming a carbene (*m/z* 108.0445), which can further rearrange to the isobaric aldehyde by intramolecular H-shift.[34] Further structural analyses are needed to confirm the exact identity of the third diol.

The NNK metabolite, α-OH-methyl-NNAL-Gluc **(14)** is related to the glucuronide of α-OH-methyl-NNK (Figure 1, **7**), which was characterized as a metabolite of NNK in the rat a number of years ago.[14] Therefore, we expected that the analogous glucuronide of α-OH-methyl-NNAL (Figure 5, **14**) would be formed and d_0 and d_4-*m/z* metabolite pair with the correct masses of d_0-α-OH-methyl-NNAL-Gluc, *m/z* 402.1508 and d_4-α-OH-methyl-NNAL-Gluc, *m/z* 406.1759 was detected eluting 3.2 min earlier than the α-OH-methyl-NNK-Gluc (Figure S2a, b). The fragmentation pattern of this new metabolite was analogous to that of the well-characterized fragmentation pattern of α-OH-methyl-NNK-Gluc (Figure S2c, d). Pairs of fragment ions separated by 4 Da due to the 4 deuterium were observed in the MS^2 of the two compounds. The proposed structures of the fragment ions in the MS^2 spectra of these compounds are presented in Figure S2c, d. The relative ion abundance of α-OH-methyl-NNAL-Gluc was at least 5 times lower than the α-OH-methyl-NNK-Gluc.

The NNK metabolite, nitro-NK-*N*-oxide **(15)** identified in the rat is characterized by d_0- *m/z* 240.0977 and d_4-*m/z* 244.1229 and t_R: 14.7 min. The MS^2 spectra showed fragment ions consistent with the structures shown in Figure S3b. The fragmentation data of this compound is similar to that of NNK-*N*-oxide. However, the loss of 62.9956 Da (HNO_3) from the molecular ion peak (*m/z* 240.0977) is observed for this compound, whereas the loss of 47.0007 Da (HNO_2) is observed in the MS^2 of NNK-*N*-oxide. We hypothesized that this compound could be a hydroxylated NNK-*N*-oxide or a nitroamine, wherein the nitroso group is further oxidized to NO_2. This compound was found to be a minor contaminant of the NNK-*N*-oxide standard. Therefore, we isolated it from a solution of the synthetic NNK-*N*-oxide and obtained NMR spectra (Figure S3c). The NMR (^{1}H-NMR, ^{1}H-^{1}H COSY) data were consistent with the nitroamine of NNK-*N*-oxide (Figure 5, **15**; Figure S3d, e).

Author Manuscript Author Manuscript Author Manuscript Author Manuscript

A second, related novel metabolite, nitro-NAL-*N*-oxide was observed with *m/z* 242.1135) **(16).** The MS^2 fragmentation data for this compound is consistent with a nitroamine of NNAL-*N*-oxide (Figure 5, **16**). The MS^2 fragmentation of *m/z* 242.1135 has many features common to the fragmentation of NNAL-*N*-oxide, except that a loss of 62.9956 Da (HNO_3) from the molecular ion peak, *m/z* 242.1135 (Figure S4b) was observed, not the loss of 47.0007 Da (HNO_2) that was observed for the MS^2 of NNAL-*N*-oxide.

Three metabolites with *m/z* 226.1186 were observed. This mass is that of either a hydroxylated NNAL metabolites (OH-NNAL) or the most abundant NNK metabolite present in rat urine, NNAL-*N*-oxide (Figure 1, 3). The NNAL-*N*-oxide (t_R= 12.8 min) was detected at relatively high levels and the two additional compounds were present in lower abundance (Table 1). We hypothesized these compounds are hydroxylated NNAL metabolites, OH-NNAL 2 (**17**) and OH-NNAL 1 (**20**). The major MS^2 fragment of OH-NNAL 2 (**17**) is *m/z* 135.0678 (Figure 5Sb, Panel III). This fragment is not present in the fragmentation spectrum of NNAL-*N*-oxide standard (Figure S5d, Panel I), which has two characteristic fragments, *m/z* 161.10735 and *m/z* 179.1179. An EIC of *m/z* 135.0678 and *m/z* 179.1184 clearly illustrated the presence of two additional metabolites (t_R: 13.6 and 14.3) that are isobaric with NNAL-*N*-oxide. Hydroxylation of NNAL can occur in α, β, or γ positions from the N-nitroso group and on the pyridine ring. We ruled out hydroxylation on the pyridine ring since the d_4-NNK is deuterated on the pyridine ring and no loss of deuterium was observed. α-hydroxylation is the main pathway involved in the metabolic activation of NNK, however α-OH NNK and α-OH NNAL are unstable and typically detected as their glucuronides or as metabolites of non-enzymatic degradation products. To confirm the identity of the hydroxylated NNAL, a synthetic standard of β-OH NNAL was prepared. LC/MS and co-injection experiments confirmed that no β-OH NNAL was present in the rat urine. The hydroxylated NNAL metabolites (**17)** and (**20)** did not co-elute with β-OH NNAL (Figure S5e). We hypothesized that OH-NNAL 2 (**17)** could be γ-OH NNAL as the MS^2 fragmentation data are consistent with a structure with the hydroxyl group in the γ position (Figure 5, **17**). Unfortunately, OH-NNAL 1 (**20**) partially co-elutes with another metabolite, NNAL-*N*-oxide, therefore a clean MS^2 spectra was not obtained for this compound limiting our ability to hypothesize its structure. Further confirmation of the structures of the two newly identified hydroxylated NNAL metabolites is underway.

In addition to the metabolites mentioned above, our method allowed the detection of N-acetylcysteine-PHB (NAC-PHB) (18a, 18b, 18c) in the urine of treated rats. Figure S6a shows the EICs of *m/z* 313.1214 (d_0) and *m/z* 317.1464 (d_4) showing three distinct peaks at retention times of: 16.6 min, 17.2 min, and 17.9 min, which could correspond to three possible isomers. The MS^2 spectra of the chromatographic peaks at 17.2 min and 17.9 min showed similar fragment ions and are consistent with isomers of N-acetylcysteine-PHB (Figure S6b–c). Because the ion abundance of the chromatographic peak at 16.6 min is too low, we were not able to get a good MS^2 mass spectral data for this compound. The two isomers of PHB-NAC metabolites shown in Figure S6d have been previously identified in rat hemoglobin,[35] while the identity of the third isomer needs to be elucidated. An unknown metabolite (*m/z* 214.0893), which we hypothesized to contain a thiol group based on its measured high-resolution accurate mass was also identified. This metabolite could be a

Author Manuscript Author Manuscript Author Manuscript Author Manuscript

breakdown product of in-source decay (ISD), and the exact identity of the precursor compound still needs to be elucidated (Table S11; Figure S7a,b). Lastly, another unknown compound (**21**) was also detected and characterized by the initial loss of HNO_2 (Table 1, Figure S8a, b). Based on the measured high-resolution accurate mass of its precursor $[M+H]^+$ and MS^2 fragment ions, we proposed that this compound could be a methoxylated NNK metabolite, however, the exact identity of this unknown compound needs further investigation.

Identification of in-source decay ions (ISD), artifacts, metabolite adducts, ion clusters (C) and dimers (D).

A number of *m/z* pairs corresponding to ISDs, adducts, and artefacts from sample preparation conditions were also identified (Table S11). The detection of ISD ions, with exact retention times of the precursor ions for several known metabolites (e.g. NNAL-*N*-oxide (**3**), NNK-*N*-oxide (**4**), NNAL (**2**), and NNK (**1**); Table S11), further confirmed their identities. Artefactual formation of NNK metabolites generated during sample cleanup was also identified and is a critical finding for the design of suitable sample cleanup procedures for the quantitation of these metabolites. Previous studies have quantified intact NNAL glucuronides in human urine and have used the SRM transition *m/z* 386→*m/z* 210.[21] However, here we have identified a methyl ester of NNAL-O-Gluc (**6**, *m/z* 400.1713). We have confirmed that the artefactual formation of the methyl ester occurs with a synthetic standard of NNAL-O-Gluc, which has been processed by the sample enrichment strategy illustrated in Figure 2b (Figure S9b). If some of the glucuronides are esterified as a result of sample preparation conditions, quantitation of these compounds would be affected, and amounts underestimated. This artefactual derivatization was also observed with other glucuronidated NNK metabolites such as α-OH-methyl-NNK-Gluc (**7**).

Finally, our workflow revealed extensive dimerization of NNK metabolites and ion clustering with solvent molecules such as methanol, and other high-abundant endogenous compounds present in the sample during ESI-MS analysis (Table S11). For example, N-oxides in general can form extensive dimerization during ESI-MS.[36,37] Clusters of NNAL-*N*-oxide and methyl guanosine was observed at *m/z* 523.2259 (d_0) and *m/z* 527.2513 (d_4) (Figure S10, Panel I and II). Upon HCD, the intact precursor and fragment ions from both NNAL-*N*-oxide (*m/z* 226.11858) and methyl guanosine (*m/z*, 298.11444) were observed in the MS^2 spectra (Figure S10c). This cluster disappeared when the sample was diluted 1000 times, which indicates that this clustering is due to the high-concentration of NNAL-*N*-oxide and methyl guanosine in the urine samples (Figure S10d, Panel I and II).

Relative distribution of NNK metabolites after phenobarbital (PB) induction.

One of the future goals of this work is to be able to use this workflow to characterize all NNK metabolites in humans to predict lung cancer risk and susceptibility among smokers. We hypothesized that genetic differences would result in variations in the capacity to activate and detoxify carcinogens, and therefore will result in differing levels of NNK metabolites in biological fluids. To mimic probable dysregulation and disparities in the metabolic enzyme activities, we induced the enzymes responsible for NNK metabolism using PB. Because our focus is on the identification and quantitation of NNK-specific

Author Manuscript Author Manuscript Author Manuscript Author Manuscript

metabolites in humans, we used those metabolites containing the nitroso group (Figure 1), as other metabolites of NNK (non-nitroso containing) may be derived from nicotine. Figure 6 shows the NNK metabolic profiles of Rat A before and after PB induction. The levels of several metabolites changed with PB induction. For example, the level of NNK (**1**) after induction decreased only slightly (+PB/-PB = 0.8), but dramatic differences were observed in the case of NNAL (**2**), NNAL-O-Gluc (**3**), and α-OH-methyl-NNK-Gluc (**7**). The NNAL levels decreased by two-fold, while the levels of NNAL-O-Gluc and α-OH-methyl-NNK-Gluc increased after PB induction, which is consistent with increased enzyme activity of UGTs responsible for the glucuronidation of various xenobiotics. These results are consistent with previous studies on rats upon induction of PB or 3-methylcholantrene (MC).[14,15] The ratio of NNAL (+PB/-PB = 0.5) and α-OH-methyl-NNK-Gluc (+PB/-PB = 2.7) using MS-based absolute quantitation (data not shown) is in agreement with the ratio of NNAL (+PB/-PB = 0.5) and only slightly with α-OH-methyl-NNK-Gluc (+PB/-PB = 4.1) obtained using our LC-MS^2 approach.

CONCLUSIONS

We have used an *in vivo* isotope labeling approach using d_0-NNK and d_4-NNK for the comprehensive profiling and simultaneous identification of known and unknown NNK metabolites in rats. The combined sample preparation, HR-AM LC/MS, and data analysis workflow presented here revealed and confirmed known NNK metabolites as well as *m/z* pairs corresponding to new and novel NNK metabolites. Several proposed NNK metabolites including the 1,3-Diol (**13)**; α-OH-methyl-NNAL-Gluc (**14**); nitro-NK-*N*-oxide (**15**); nitro-NAL-*N*-oxide (**16**); γ-OH NNAL (**17**); and three N-acetylcysteine (NAC) metabolites (**18a-c**) were characterized for the first time in rat urine. Our current workflow detected metabolites that could have been missed using only targeted MS-based approaches. In addition, we detected in-source decay products (ISD), salt adducts, artefacts, and extensive formation of ion clusters and dimers. The identification of the source of these compounds is necessary to develop an accurate method for NNK metabolite detection. This strategy will be used to monitor and quantify NNK metabolites in human urine using a panel of metabolite biomarkers to assess carcinogen uptake, metabolic activation and detoxification, and ultimately for the evaluation of lung cancer risk and identification of susceptible smokers. The characterized rat urine from [pyridine-d_4]NNK treated rats in this study may be used as internal standards for the relative quantitation of NNK metabolism in humans. Finally, the custom script reported here for the automated d_0-d_4 *m/z* pair peak detection could be integrated into the Compound Discoverer software package to allow users to interrogate high-resolution orbitrap-acquired mass spectral data using stable isotope labeling approaches.

Supplementary Material

Refer to Web version on PubMed Central for supplementary material.

ACKNOWLEDGMENTS

This work was supported by grant CA-138338 from the National Cancer Institute. R.D. was partially supported by the 2017 American Society for Mass Spectrometry Postdoctoral Career Development Award. Mass spectrometry

Author Manuscript Author Manuscript Author Manuscript Author Manuscript

was carried out in the Analytical Biochemistry Shared Resource of the Masonic Cancer Center, University of Minnesota, funded in part by Cancer Center Support Grant CA-077598. Salary support for P.W.V. was provided by the U.S. National Institutes of Health and National Cancer Institute [Grant R50-CA211256]. We thank Dr. Stephen Hecht (University of Minnesota), Dhimant Desai, Ph.D. and Shantu Amin, Ph.D. (Penn State Milton S. Hershey Medical Center, Hershey, PA) for providing the synthesized β-OH NNK, Drs. Lisa Peterson and Irina Stepanov for their helpful comments on this work, and Robert Carlson for editorial assistance.

Abbreviations:

NNK
4-(Methylnitrosamino)-1-(3-pyridyl)-1-butanone

NNAL
4-(Methylnitrosamino)-1-(3-pyridyl)-1-butanol

NNK-*N*-oxide
4-[Methyl(nitroso)amino]-1-(1-oxido-3-pyridinyl)-1-butanone

NNAL-*N*-oxide
4-[Methyl(nitroso)amino]-1-(1-oxido-3-pyridinyl)-1-butanol

α-OH-methyl-NNK-Gluc
3,4,5-trihydroxy-6-((nitroso(4-oxo-4-(pyridin-3-yl)butyl)amino)methoxy)tetrahydro-2*H*-pyran-2-carboxylic acid

α-OH-methyl-NNAL-Gluc
3,4,5-Trihydroxy-6-(((4-hydroxy-4-(pyridin-3-yl)butyl)(nitroso)amino)methoxy)tetrahydro-2H-pyran-2-carboxylic acid

NNAL-O-Gluc
4-(Methylnitrosamino)-1-(3-pyridyl)-1-butanol-O-glucuronide

nitro-NK-N-oxide
3-(4-(Methyl(nitro)amino)butanoyl)pyridine 1-oxide; nitro-NAL-*N*-oxide, 3-(1-Hydroxy-4-(methyl(nitro)amino)butyl)pyridine 1-oxide

γ-OH NNAL
N-(3,4-Dihydroxy-4-(pyridin-3-yl)butyl)-*N*-methylnitrous amide

β-OH NNK
3-Hydroxy-4-[methyl(nitroso)amino]-1-(pyridine-3-yl)butan-1-one

β-OH NNAL
4-[Methyl(nitroso)amino]-1-(pyridine-3-yl)butane-1,3-diol

β-OH NNK-*N*-oxide
3-Hydroxy-4-[methyl(nitroso)amino]-1-(1-oxidopyridin-3-yl)butan-1-one

6-OH NNK
4-(Methylnitrosamino)-1-[3-(6-hydroxypyridyl)-1-butanone

Author Manuscript Author Manuscript Author Manuscript Author Manuscript

HPB
4-Hydroxy-1-(3-pyridyl)-1-butanone

HPB-Gluc
4-Hydroxy-1-(3-pyridyl)-1-butanone glucuronide

HPBA
4-Hydroxy-4-(3-pyridyl)-butyric acid

OPBA
4-Oxo-4-(3-pyridyl)butyric acid

1,4-Diol
4-Hydroxy-1-(3-pyridyl)-1-butanol

1,3-Diol
3-Hydroxy-1-(3-pyridyl)-1-butanol

NAC
N-acetylcysteine

PB
Phenobarbital

UDPGT
UDP-glucuronosyl transferase

REFERENCES

(1). Siegel RL; Miller KD; Jemal A CA Cancer J Clin 2017, 67, 7–30. [PubMed: 28055103]
(2). Hecht SS Nat Rev Cancer 2003, 3, 733–744. [PubMed: 14570033]
(3). Hecht SS Chem Res Toxicol 2008, 21, 160–171. [PubMed: 18052103]
(4). Rodriguez-Antona C; Gomez A; Karlgren M; Sim SC; Ingelman-Sundberg M Hum Genet 2010, 127, 1–17. [PubMed: 19823875]
(5). Schwartz AG; Prysak GM; Bock CH; Cote ML Carcinogenesis 2007, 28, 507–518. [PubMed: 17183062]
(6). Taioli E Carcinogenesis 2008, 29, 1467–1474. [PubMed: 18550573]
(7). Balbo S; Johnson CS; Kovi RC; James-Yi SA; O'Sullivan MG; Wang M; Le CT; Khariwala SS; Upadhyaya P; Hecht SS Carcinogenesis 2014, 35, 2798–2806. [PubMed: 25269804]
(8). Hecht SS; Carmella SG; Foiles PG; Murphy SE; Peterson LA Environ Health Perspect 1993, 99, 57–63. [PubMed: 8319660]
(9). Hecht SS; Peterson LA; Spratt TE IARC Sci Publ 1994, 91–106. [PubMed: 7806343]
(10). Hecht SS; Carmella SG; Murphy SE; Akerkar S; Brunnemann KD; Hoffmann D N Engl J Med 1993, 329, 1543–1546. [PubMed: 8413477]
(11). Hecht SS; Young R; Chen CB Cancer Res 1980, 40, 4144–4150. [PubMed: 7471055]
(12). Hecht SS Proc Soc Exp Biol Med 1997, 216, 181–191. [PubMed: 9349687]
(13). Peterson LA; Ng DK; Stearns RA; Hecht SS Chem Res Toxicol 1994, 7, 599–608. [PubMed: 7841337]
(14). Murphy SE; Spina DA; Nunes MG; Pullo DA Chem Res Toxicol 1995, 8, 772–779. [PubMed: 7548761]

Author Manuscript Author Manuscript Author Manuscript Author Manuscript

(15). Murphy SE; Nunes MG; Hatala MA Chem Biol Interact 1997, 103, 153–166. [PubMed: 9134006]

(16). Maertens LA; Upadhyaya P; Hecht SS; Zimmerman CL Drug Metab Dispos 2010, 38, 752–760. [PubMed: 20159989]

(17). Jalas JR; Ding X; Murphy SE Drug Metab Dispos 2003, 31, 1199–1202. [PubMed: 12975327]

(18). Jalas JR; McIntee EJ; Kenney PM; Upadhyaya P; Peterson LA; Hecht SS Chem Res Toxicol 2003, 16, 794–806. [PubMed: 12807363]

(19). Schrader E; Hirsch-Ernst KI; Richter E; Foth H Naunyn Schmiedebergs Arch Pharmacol 1998, 357, 336–343. [PubMed: 9550307]

(20). Carmella SG; Le Ka KA; Upadhyaya P; Hecht SS Chem Res Toxicol 2002, 15, 545–550. [PubMed: 11952341]

(21). Yao L; Zheng S; Guan Y; Yang J; Liu B; Wang W; Zhu X Anal Chim Acta 2013, 788, 61–67. [PubMed: 23845482]

(22). Park SL; Carmella SG; Ming X; Vielguth E; Stram DO; Le Marchand L; Hecht SS Cancer Epidemiol Biomarkers Prev 2015, 24, 561–569. [PubMed: 25542827]

(23). Leeming MG; Isaac AP; Pope BJ; Cranswick N; Wright CE; Ziogas J; O'Hair RA; Donald WA Anal Chem 2015, 87, 4104–4109. [PubMed: 25818563]

(24). Bueschl C; Kluger B; Neumann NKN; Doppler M; Maschietto V; Thallinger GG; Meng-Reiterer J; Krska R; Schuhmacher R Anal Chem 2017, 89, 9518–9526. [PubMed: 28787149]

(25). Capellades J; Navarro M; Samino S; Garcia-Ramirez M; Hernandez C; Simo R; Vinaixa M; Yanes O Anal Chem 2016, 88, 621–628. [PubMed: 26639619]

(26). Huang X; Chen YJ; Cho K; Nikolskiy I; Crawford PA; Patti GJ Anal Chem 2014, 86, 1632–1639. [PubMed: 24397582]

(27). Kessler N; Walter F; Persicke M; Albaum SP; Kalinowski J; Goesmann A; Niehaus K; Nattkemper TW PLoS One 2014, 9, e113909.

(28). Chokkathukalam A; Jankevics A; Creek DJ; Achcar F; Barrett MP; Breitling R Bioinformatics 2013, 29, 281–283. [PubMed: 23162054]

(29). Smith CA; O'Maille G; Want EJ; Qin C; Trauger SA; Brandon TR; Custodio DE; Abagyan R; Siuzdak G Ther Drug Monit 2005, 27, 747–751. [PubMed: 16404815]

(30). Kotandeniya D; Carmella SG; Pillsbury ME; Hecht SS J Chromatogr B Analyt Technol Biomed Life Sci 2015, 1007, 121–126.

(31). Cao B; Zhang Q; Ji H; Liu J; Lang H; Feng M; Zhang J Anal Bioanal Chem 2014, 406, 4465–4471. [PubMed: 24817362]

(32). Hu CW; Hsu YW; Chen JL; Tam LM; Chao MR Arch Toxicol 2014, 88, 291–299. [PubMed: 24057573]

(33). Spratt TE; Peterson LA; Confer WL; Hecht SS Chem Res Toxicol 1990, 3, 350–356. [PubMed: 2133084]

(34). Buck H International Journal of Quantum Chemistry 2012, 112, 3711–3719.

(35). Carmella SG; Kagan SS; Spratt TE; Hecht SS Cancer Res 1990, 50, 5453–5459. [PubMed: 2201436]

(36). Ibrahim H; Couderc F; Perio P; Collin F; Nepveu F Rapid Commun Mass Spectrom 2013, 27, 621–628. [PubMed: 23413221]

(37). Butler M; Arroyo Mañez P; Cabrera GM J Mass Spectrom 2010, 45, 536–544. [PubMed: 20446312]

Author Manuscript Author Manuscript Author Manuscript Author Manuscript

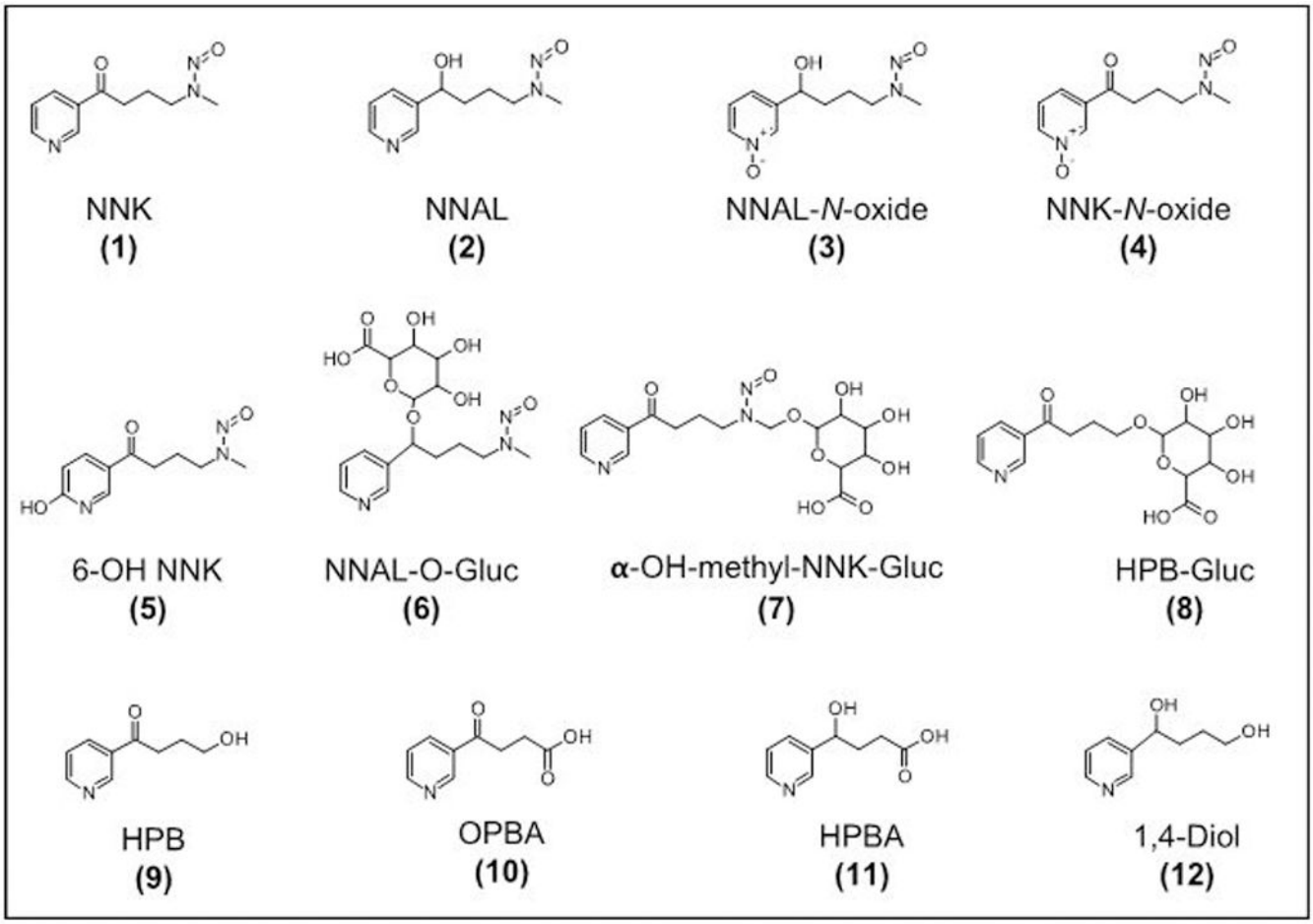

Figure 1.
Structures of NNK and its known metabolites as determined in laboratory animals.

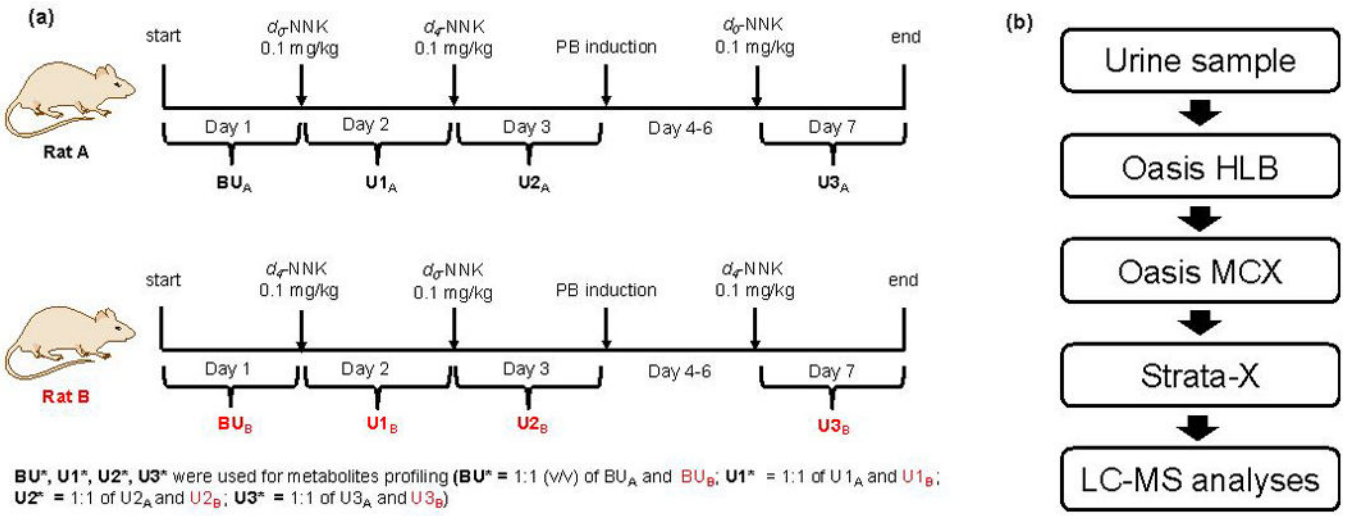

Figure 2.

(a) Experimental scheme for characterizing NNK metabolites in rats. (b) Optimized sample enrichment strategy wherein most of the known NNK metabolites in PB-induced rat urine were detected.

Author Manuscript Author Manuscript Author Manuscript Author Manuscript

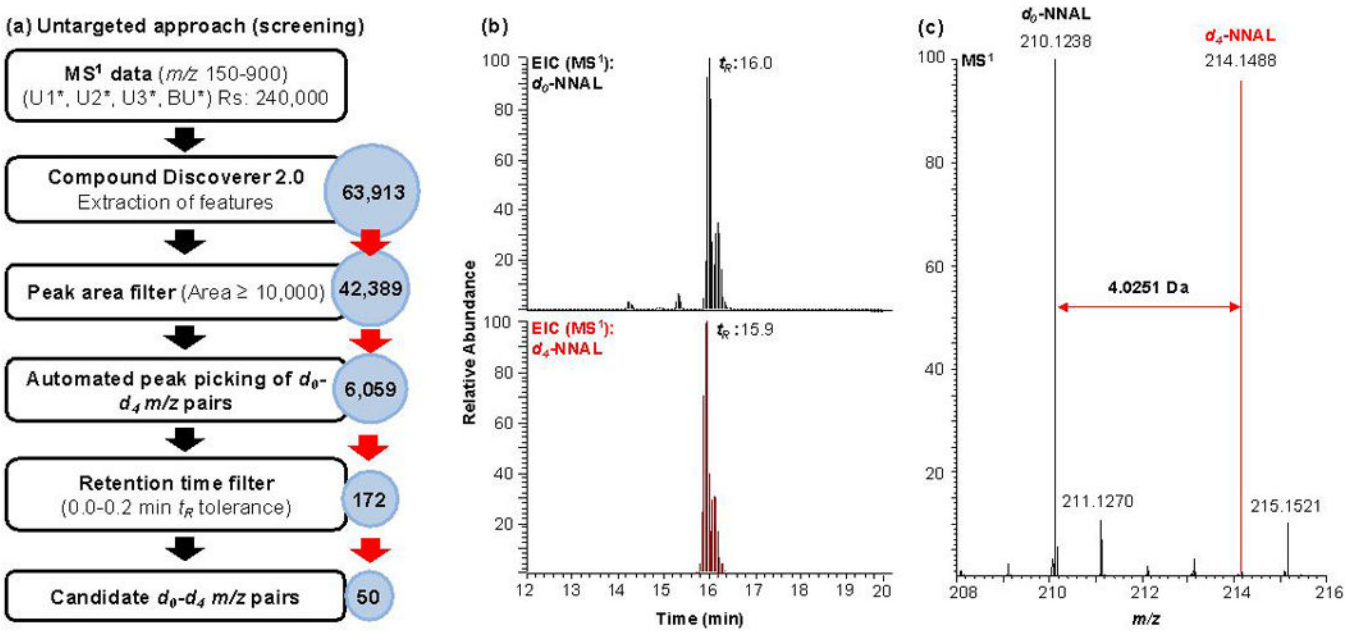

Figure 3.

LC/MS and data analysis workflow for the comprehensive profiling of all known and unknown NNK metabolites in rats. (a) Untargeted MS-based profiling approach. Features extracted using Compound Discoverer from high-resolution full scan data (Rs=240,000) were subjected to a series of filters. The peak area filter was used to exclude low abundant features (Peak area <10,000) before the automatic peak picking of *m/z* pairs using a custom script. The resulting list of *m/z* pairs were then filtered using a specified retention window (0–0.2 min) resulting to a list of candidate *m/z* pairs/metabolites. (b) Representative extracted ion chromatogram (EIC) of NNAL, a major NNK metabolite, from the full scan mass spectral data. (c) MS^1 spectrum of d_0-NNAL and d_4-NNAL.

Author Manuscript Author Manuscript Author Manuscript Author Manuscript

Author Manuscript Author Manuscript Author Manuscript Author Manuscript

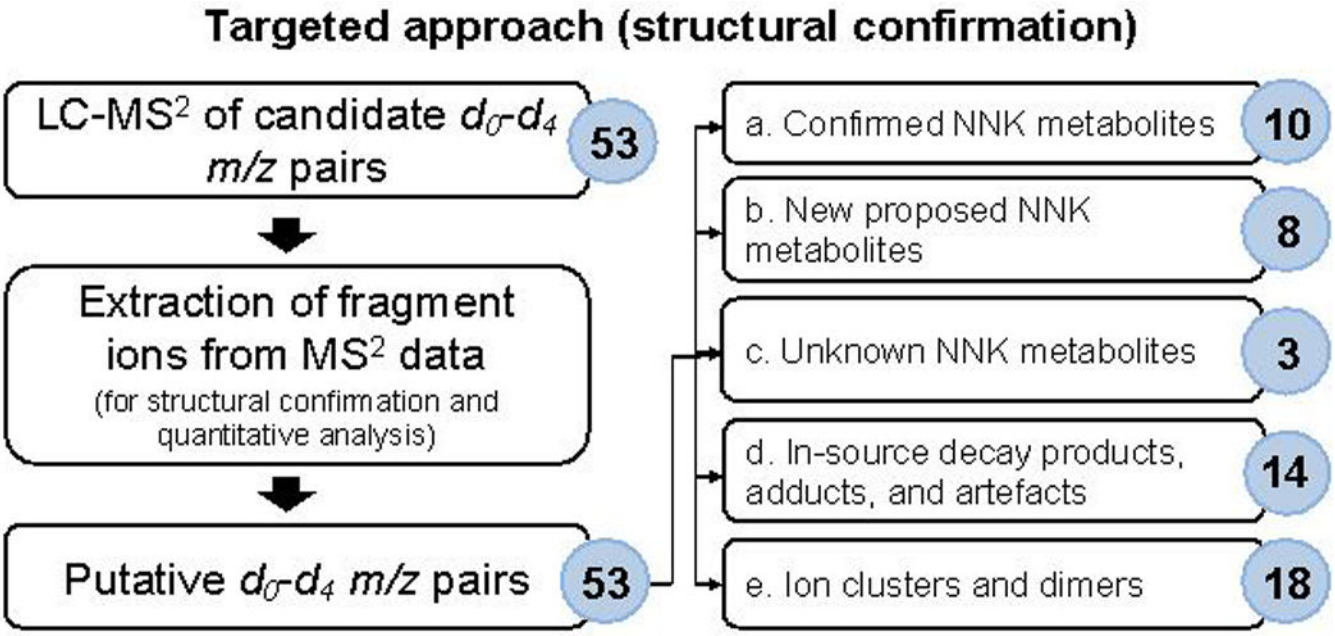

Figure 4.

Targeted MS-based approach using LC-MS^2 for structural confirmation of the candidate *m/z* pairs/metabolites identified in the untargeted profiling approach. The identities of several analytes were confirmed by comparing their t_R and MS^2 fragmentation pattern to that of synthetic standards. While unknown metabolites were identified using their MS^2 mass spectral fragmentation data and database search in METLIN when possible.

Author Manuscript Author Manuscript Author Manuscript Author Manuscript

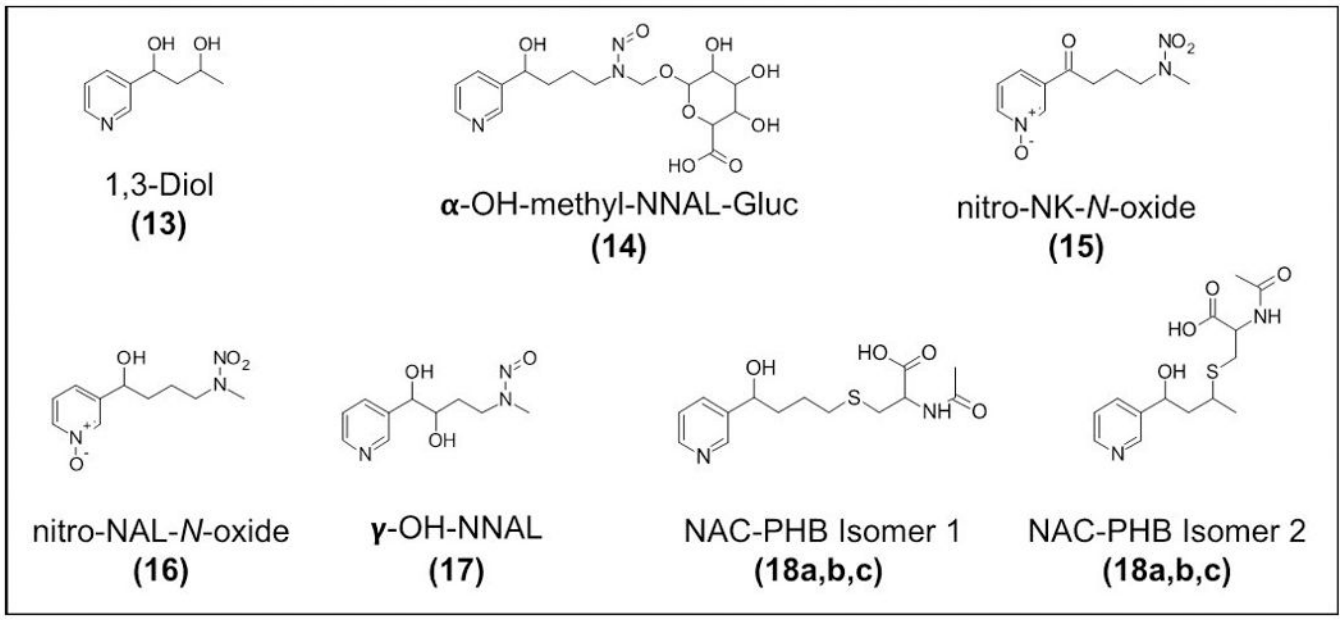

Figure 5.

Proposed structures of new and novel NNK metabolites identified in rats including the 1,3-Diol (**13)**; α-OH-methyl-NNAL-Gluc (**14**); nitro-NK-*N*-oxide (**15**); nitro-NAL-*N*-oxide (**16**); γ-OH NNAL (**17**); and three N-acetylcysteine (NAC) metabolites (**18a, 18b, 18c**).

Author Manuscript Author Manuscript Author Manuscript Author Manuscript

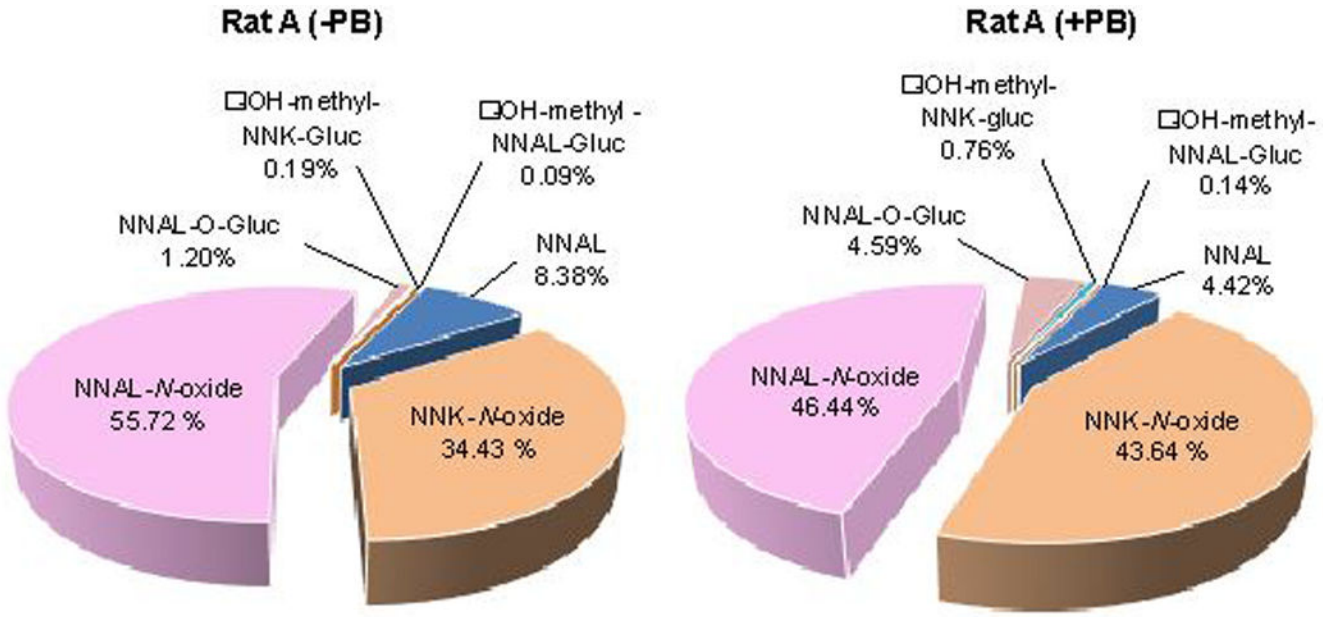

Rat A	(-) PB (%)	(+) PB (%)	(+PB)/(-PB)
NNAL **(2)**	8.38	4.42	0.5
NNAL-*N*-oxide **(3)**	55.72	46.44	0.8
NNK-*N*-oxide **(4)**	34.43	43.64	1.3
NNAL-O-Gluc **(6)**	1.20	4.59	3.8
OH-methyl-NNK-Gluc **(7)**	0.19	0.76	4.1
OH-methyl-NNAL-Gluc **(13)**	0.09	0.14	1.6

Figure 6.
Relative distribution of selected nitroso-containing NNK metabolites in rats before and after induction by PB.

Author Manuscript Author Manuscript Author Manuscript Author Manuscript

Table 1.

Identification of confirmed NNK metabolites, new proposed NNK metabolites, and unknown NNK metabolites using untargeted (UT) and targeted (T) mass spectrometry-based methods. Structural characterization by mass spectrometry (MS) was performed using the measured high-resolution accurate precursor masses in the full scan (MS^1) and MS^2 mass spectral data and when possible, comparing with standards. For NMR, ^{1}H-NMR and ^{1}H-^{1}H COSY were performed.

d_0 m/z	d_4 m/z	d_0 t_R (min)	d_4 t_R (min)	Description	MS method (Untargeted, UT; Targeted, T)	Structural Confirmation
Confirmed metabolites						
182.0811	186.1061	8.2	8.1	HPBA **(11)**	UT, T	Synthetic standard (t_R, MS)
386.1556	390.1806	12.6	12.6	NNAL-O-Gluc **(6)**	UT, T	Synthetic standard (t_R, MS)
226.1184 *	230.1434	12.8	12.7	NNAL-*N*-oxide **(3)**	UT, T	Synthetic standard (t_R, MS)
342.1180	346.1430	12.9	12.9	HPB-Gluc **(8)**	UT, T	Literature (MS)
180.0656	184.0906	13.0	12.9	OPBA **(10)**	UT, T	Synthetic standard (t_R, MS)
224.1032	227.1221 (d_3)	14.1	14.0	6-OH NNK **(5)**	T	Literature (MS)
224.1032	228.1280	14.1	14.0	NNK-*N*-oxlde **(4)**	UT, T	Synthetic standard (t_R, MS)
400.1350	404.1601	14.5	14.5	**α**-OH-methyl-NNK-Gluc **(7)**	UT, T	Literature (MS)
168.1019	172.1269	14.3	14.2	1,4-Diol (Diol 1) **(12)**	UT, T	Synthetic standard (t_R, MS)
210.1243	214.1486	16.0	15.9	NNAL **(2)**	UT, T	Synthetic standard (t_R, MS)
166.0863	170.1113	16.7	16.7	HPB **(9)**	T	Literature (MS)
208.1081	212.1331	17.5	17.4	NNK **(1)**	UT, T	Synthetic standard (t_R, MS)
New proposed metabolites						
168.1019	172.1269	15.6	15.5	1,3-Diol (Diol 2) **(13)**	UT, T	Synthetic standard (t_R, MS)
402.1508	406.1759	11.3	11.2	**α**-OH-methyl-NNAL-Gluc **(14)**	UT, T	MS
240.0977	244.1229	14.7	14.7	nitro-NK-*N*-oxide **(15)**	UT, T	MS, NMR
242.1135	246.1386	13.6	13.5	nitro-NAL-*N*-oxide **(16)**	T	MS
226.1185	230.1437	13.9	13.9	**γ**-OH NNAL (OH-NNAL 2) **(17)**	UT, T	MS
313.1214	317.1462	15.8	15.8	NAC-PHB 1 **(18a)**	UT, T	MS
313.1213	317.1465	16.4	16.3	NAC-PHB 2 **(18b)**	UT, T	MS
313.1214	317.1465	17.2	17.2	NAC-PHB 3 **(18c)**	UT, T	MS
Unknown metabolites						
168.1019	172.1270	16.1	16.0	Unknown 1 (Diol 3) **(19)**	UT, T	Unknown
226.1185	230.1437	13.6	13.5	Unknown 2 (OH-NNAL 1) **(20)**	T	Unknown
254.1135	258.1385	14.1	14.0	Unknown 3 **(21)**	UT, T	Unknown

* *m/z* 226.1185, t_R12.8 min (Table 1, confirmed metabolites) vs. t_R:13.4 min (Figure S5a, Panel III)